

1 The effect of organoclay addition on the properties of an acrylate based, thermally activated
2 shape memory polymer.

3 Michael J. Barwood^{a,1}, Chris Breen^{a,*}, Francis Clegg^a, Carol L. Hammond^b

4 ^aMaterials and Engineering Research Institute, Sheffield Hallam University, Sheffield, S1 1WB, UK

5 ^bMultipackaging Solutions, Millenium Way West, Phoenix Centre, Nottingham, NG6 6AW, UK

6
7 ABSTRACT

8
9 Shape Memory Polymers ([SMPSMPs](#)) exhibit the intriguing ability to change back from an
10 intermediate, deformed shape back to their original, permanent shape. In this contribution a
11 systematic series of t-butylacrylate-co-poly(ethyleneglycol) dimethacrylate (tBA-co-
12 PEGDMA) polymers have been synthesised and characterised prior to incorporation of
13 organoclay. Increasing the poly(ethyleneglycol) dimethacrylate (PEGDMA) content in
14 increments of 10% increased the storage modulus from 2005 to 2250 MPa, reduced the
15 glass transition temperature from +41 to -26°C and reduced the intensity of the associated
16 tan δ peak. The tBA-co-PEGDMA crosslinked networks displayed useful shape memory
17 properties up to PEGDMA contents of 40 %. Above this PEGDMA percentage the
18 materials were prone to fracture and too brittle for a realistic assessment of their shape
19 memory capability. The system containing 90% t-butylacrylate (tBA) and 10% PEGDMA
20 was selected as the host matrix to investigate how the incorporation of 1 to 5 mass% of a
21 benzyl tallow dimethylammonium-exchanged bentonite, (BTDB) influenced the shape
22 memory properties. X-ray diffraction data confirmed that BTDB formed a microcomposite
23 in the selected matrix and exerted no influence on the storage modulus, rubbery modulus,
24 glass transition temperature, T_g , or the shape or intensity of the tan δ peak of the host
25 matrix. Therefore, it was anticipated that the presence of BTDB would have no effect,
26 positive or negative, nor on the shape memory properties of the host matrix. However, it
27 was found that the incorporation of clay, especially at the 1 mass% level, significantly
28 accelerated the speed, compared ~~to~~ with the clay-free [SMPSMPs](#), at which the
29 microcomposite returned to the original, permanent shape. This accelerated return to the
30 permanent shape was also observed when the microcomposite was coated onto a 100 μ m
31 PET film.

32
33 *Keywords*

34 *Shape memory polymer, nanocomposite, organoclay, polyacrylate*

35
36 **Corresponding Author:**

37 Professor Chris Breen, Materials and Engineering Research Institute, Sheffield Hallam University, Sheffield
38 S1 1WB, UK. Phone +44-1142253008. E-mail: c.breen@shu.ac.uk

39 **Contact details for other authors:**

40 Dr. Francis Clegg, Materials and Engineering Research Institute, Sheffield Hallam University, Sheffield S1
41 1WB, UK. Phone +44-1142253062. E-mail: f.clegg@shu.ac.uk

42 Dr. Michael Barwood, Materials and Engineering Research Institute, Sheffield Hallam University, Sheffield
43 S1 1WB, UK. Phone +44-1142253008. E-mail: m.barwood@lboro.ac.uk

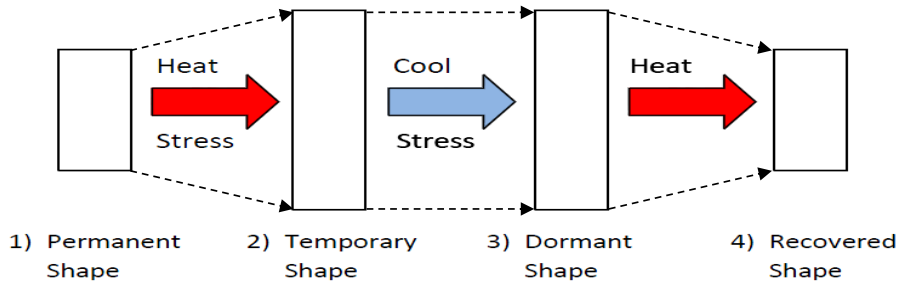
44 Carol Hammond, Multipackaging Solutions, Millenium Way West, Phoenix Centre, Nottingham, NG6 6AW,
45 UK. carol.hammond@multipkg.com

46

47 ¹Dr. Michael Barwood, Centre for Sustainable Manufacturing and Recycling Technologies, Wolsol School of
48 Mechanical and Manufacturing Engineering, Loughborough University, Leicestershire, LE11 3TU, UK.

49
50 **1. Introduction.**

51 Shape memory polymers ([SMPSMPs](#)) have the ability to store a permanent shape and be
52 deformed into a temporary shape by applying an external stress and temperature. This
53 temporary shape is stored by cooling into the dormant shape, in which it remains, until [it is](#)
54 encouraged to return to its original, permanent shape ([FigureFig. 1](#)). The transformation from
55 the stressed temporary shape back to the permanent, stress-free shape is usually triggered by
56 thermal (Liff et al., 2007), electrical (Liu et al., 2009), or other environmental stimuli e.g. UV
57 or visible radiation (Jiang et al., 2006). This change from temporary to permanent shape is
58 essentially driven by the elastic strain stored in the dormant shape during the initial
59 deformation into the temporary shape (Liu et al., 2007).



60
61 **Fig. 1.** Schematic depiction of the unconstrained shape memory effect (SME) of a thermally
62 activated SMP.

63 The most common [SMPSMPs](#) are thermally-responsive, which means that the material is
64 deformed into its temporary shape, at one temperature and a second thermal change is
65 required to initiate the return to its original, permanent, shape. The temperature at which this
66 change in shape occurs is referred to as the transition temperature, T_{trans} , and is typically the
67 glass transition temperature, T_g , or melting transition temperature, T_m , of the polymer. The
68 unique, ‘tunable’ properties of [SMPSMPs](#) make them attractive for a number of potential
69 applications in almost every avenue of life, ranging from self-repairing car bodies (Ikematu et

70 al., 1993), kitchen utensils (Lendlein and Kelch, 2002), switches to sensors (Liu et al., 2009),
71 intelligent packaging (Behl et al., 2010), toys (Ikematu et al., 1993) and tools (Tong, 2004). A
72 significant number of studies have focussed on the use of [SMPSMPs](#) in biomedical
73 applications including sutures (Lendlein and Langer, 2002), stents (Venkatraman et al.,
74 2006), catheters (Liu et al., (2007), micro-actuators (Maitland et al., 2002) and tissue
75 scaffolds (Migneco et al., 2009). More recently, the focus has moved towards [SMPSMPs](#)
76 with two temporary shapes which transform in response to two different stimulus events
77 (Behl et al., 2010; Tao, 2010; Ge et al., 2013).

78 Two commonly adopted approaches to improve and expand the applications of [SMPSMPs](#)
79 are 1) optimise the polymer system's mechanical, thermal and shape memory properties for
80 the intended application and/or, 2) incorporate nanomaterials into the optimised polymer to
81 provide additional property enhancements. The knowledge that the incorporation of 1 to 5
82 mass% of well dispersed clay can increase both the tensile properties and the storage modulus
83 of the host polymer (Annabi-Bergaya, 2008; Utracki, 2010) means that a clay polymer
84 nanocomposite (CPN) has the potential to increase the energy stored within the temporary
85 shape of a SMP; giving it the ability to exert a stronger physical force when returning to the
86 original shape and/or transform at a faster rate. Despite their potential to improve shape
87 memory properties, clays have not been extensively studied. Most reports focus on their
88 positive influence on polyurethanes (PU) at organoclay (OC) levels of 0.5 to 2 mass% (Cao
89 and Jana, 2007; Chung et al., 2011; Haghayegh and Sadeghi, 2012) although larger quantities
90 of calcined attapulgite (Xu et al., 2009) and grafted bentonite (Wu et al., 2013) were required.
91 Rezanejad and Kokabi (2007) established that adding 12 mass% of Cloisite 15A (a
92 dihydrogenated tallow dimethyl ammonium-bentonite) increased the recovery stress by
93 200%. Finally, OC have been used to improve the shape memory properties of epoxy CPN
94 (Liu et al., 2011) and nanofoams (Quadrini et al., 2012).

95 Acrylate polymers represent an ideal system for SMP/clay studies since the copolymerization
96 of linear acrylates (mono-functional monomers) with acrylate cross linkers (multifunctional
97 monomers) yields [SMPSMPs](#) with tuneable properties that can be optimised for specific
98 applications (Safranski and Gall, 2008; Voit et al., 2010). Previous investigations by Yang et
99 al., (2007), Yakacki et al., (2008) and Ortega et al., (2008) have shown that tert-butylacrylate-
100 *co*-poly(ethylene glycol) dimethacrylate (tBA-*co*-PEGDMA) networks have shape memory
101 ability with thermal and mechanical properties that can be readily tailored. In this particular
102 example a transition temperature near 40 °C was required.

103 To our knowledge the enhancement of tBA-*co*-PEGDMA networks via incorporation of OC
104 has yet to be reported, thus this contribution represents a benchmark study designed to
105 explore the impact of clay on the properties of an optimised acrylate based SMP system. It
106 aims to identify the influence of the OC loading on a UV polymerised polyacrylate system, of
107 selected stoichiometry, and the effect on the resulting physical properties. The features under
108 investigation are; the OC loading required to influence the shape memory effect of self-
109 supporting polymer films (and when coated onto a PET substrate); the effect of OC loading
110 on the storage moduli, the glass transition temperature, and, in particular, macroscopic effects
111 including the shape fixity, the extent of shape recovery as well as the time required to return
112 to the original, permanent shape.

113 **2. Experimental**

114 *2.1 Materials*

115 The mono-functional acrylate tert-butyl acrylate (tBA), the di-functional acrylate
116 poly(ethylene glycol) dimethacrylate (PEGDMA), with an average molecular weight of 750 g
117 mol⁻¹, the photoinitiator 2,2-dimethoxy-2-phenylacetophenone (DMPA) and accelerator
118 ethyl-4-(dimethylamino) benzoate (EDB) were purchased from Sigma-Aldrich and used as

119 received. The purity of tBA was 98%, while the purities of the other reagents were $\geq 99\%$.
120 The Cloisite 10A (C10A), is a bentonite in which the resident Na^+ -cations have been replaced
121 by quaternary benzyl hydrogenated tallow dimethylammonium ions, and was supplied by
122 Rockwood Specialties Inc., UK. The substrate material used in the coating studies was a 100
123 μm thick polyethylene terephthalate (PET) film (HiFi Films Ltd.).

124 *2.2 Pre-treatment of commercial organoclay*

125 Initial attempts to fully polymerise the tBA-co-PEGDMA systems in the presence of as-
126 received C10A were unsuccessful and the excess surfactant present on C10A was identified
127 as the cause. The excess organomodifier was removed, prior to use, by dispersion in water
128 whilst stirring at 80 °C for 1 h, then filtered and washed with propan-2-ol. This was repeated
129 6 times before drying at 70°C for 4 h. The fully washed material is subsequently referred to
130 as benzyl tallow dimethylammonium-bentonite (BTDB).

131 *2.3 Preparation of polymers and PCN*

132 *2.3.1 tBA-co-PEGDMA*

133 A series of polymer networks were prepared using selected ratios of the monomers (Table 1).
134 The tBA, PEGDMA, DMPA and EDB were weighed out and added together in a glass vial,
135 wrapped in foil and the solution was magnetically stirred for 30 mins at ca. 22°C. The
136 solution was then sonicated for an additional 30 mins before photopolymerisation (see
137 [Section 2.3.3](#) below).

138 *2.3.2 tBA-co-PEGDMA/BTBD*

139 The tBA90/PEGDMA10 polymer network was used as a host matrix for selected quantities
140 of BTBD (Table 1). The procedure was similar to that described above except that the
141 mixture was stirred for 24 h at ca. 22°C, before sonication and photopolymerisation (Decker
142 et al., 2005).

143 2.3.3 Polymer Photopolymerisation

144 Photopolymerisation of stirred and ultrasonicated mixtures was carried out in a mould
 145 constructed using two ultraviolet (UV) clear glass slides, 100 x 100 x 1 mm³, to which UV
 146 clear PET film liners, 12 x 12 x 0.1 mm³ were attached so that the reaction mixture was only
 147 in contact with the PET film and the 500 µm spacer. The reaction mixtures were injected into
 148 the reaction cavity and the entire mould was placed in a UV chamber (model CL-1000
 149 ultraviolet cross-linker, λ = 254 nm, output energy = 200 mJ/cm²). The mould was turned
 150 over every 5 mins for ca. 30 mins to promote an even cure on both surfaces of the mould.

151 **Table 1.**

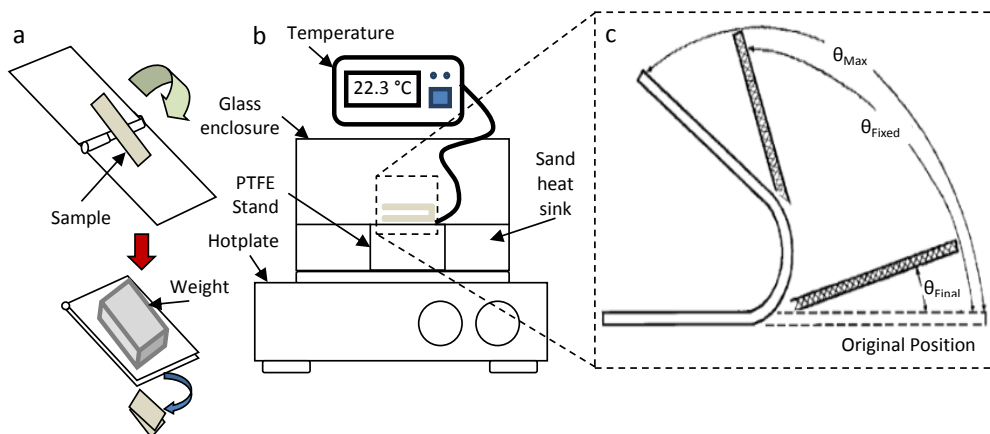
152 Sample description, notation, type, composition and clay content.

Sample Description	Sample notation in figures	Sample type	tBA / mass%	PEGDMA / mass%	BTBD / mass%
tBA100/PEGDMA0	t100/P0	Film	100	0	0
tBA90/PEGDMA10	t90/P10	Film	90	10	0
tBA80/PEGDMA20	t80/P20	Film	80	20	0
tBA70/PEGDMA30	t70/P30	Film	70	30	0
tBA60/PEGDMA40	t60/P40	Film	60	40	0
tBA15/PEGDMA85	t15/P85	Film	15	85	0
tBA0/PEGDMA100	t0/P100	Film	0	100	0
tBA90/PEGDMA10/BTBD 0	t90/P10/BTBD 0	Film	90	10	0
tBA90/PEGDMA10/BTBD 1	t90/P10/BTBD 1	Film	90	10	1
tBA90/PEGDMA10/BTBD 3	t90/P10/BTBD 3	Film	90	10	3
tBA90/PEGDMA10/BTBD 5	t90/P10/BTBD 5	Film	90	10	5
tBA90/PEGDMA10/BTBD 0	t90/P10/BTBD 0 P	Coated on PET	90	10	0
tBA90/PEGDMA10/BTBD 1	t90/P10/BTBD 1 P	Coated on PET	90	10	1

153
 154 In order to polymerise the tBA90/PEG10 mixture, with and without BTBD, onto the PET
 155 film it was applied using a meter bar, producing a ca. 30 µm thick film. The coated film was
 156 placed into a nitrogen gas filled chamber, equipped with a UV transparent window, and the
 157 entire configuration was placed into the UV chamber for ca. 30 min.

158 2.4 Characterisation Methods

159 Swelling tests and ATR-FTIR Spectroscopy were used to confirm that cross-linking had
160 taken place and DSC traces (not illustrated) confirmed that the systems were fully cured.
161 Samples (10 mm²) of tBA-co-PEGDMA network sheets were cut and weighed for their initial
162 mass, m_i , and separated into vials where they were immersed in 20 ml of propan-2-ol. The
163 samples were removed from the solvent periodically, dried lightly and weighed until an
164 equilibrium, swollen, mass, m_s , was reached. The equilibrium swelling ratio, q , was
165 calculated using the relationship, $q = m_s/m_i$.



166
167 **Fig. 2.** Schematic illustration of a) the deformation method, b) the customised shape memory
168 effect (SME) evaluation platform and c) the shape recovery process. 1) Sample was heated
169 and deformed to a temporary shape using an external force, which applied a fixed
170 compression stress. 2) The sample was fixed into its temporary shape by rapid cooling in a
171 fridge, at $3 \pm 2^\circ\text{C}$, while the external force was maintained, θ_{Max} . 3) The external force was
172 removed and θ_{Fixed}° , was assessed. 4) The sample was placed in the heated chamber at a fixed
173 temperature and recovery to θ_{Final} was recorded over time (Lin and Wu, 1992).

174

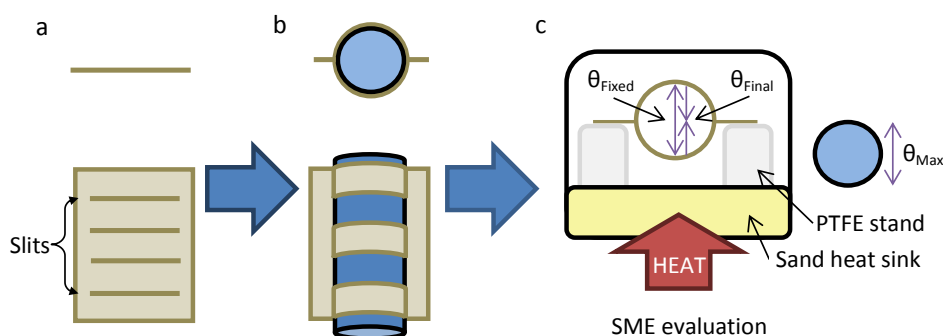
175 [The](#) ATR-FTIR spectra were collected using a Nicolet, Nexus FT-IR model at room
176 temperature. X-ray diffraction traces of cast films were recorded, over an angular range of 5
177 to $40^\circ 2\theta$, using a Philips X'Pert XRD, with a Cu X-ray source ($\lambda = 1.542 \text{ \AA}$), and a Philips
178 Miniprop detector. Dynamic Mechanical Analysis (DMA) was used to determine the

179 viscoelastic properties of the samples. A PerkinElmer model DMA8000 was employed in
180 tension mode, with no pre-load, over a temperature range of -50 to 150°C, at a frequency of 1
181 Hz. The polymer samples, $25 \times 5 (\pm 0.1) \times 0.5 \text{ mm}^3$, were equilibrated at -50°C for 3 mins
182 then raised to 90°C at a ramp rate of 3°C min^{-1} . The T_g was defined as the peak maximum of
183 the $\tan \delta$ curve. The rubbery modulus was determined from the storage modulus, when it had
184 reached a steady state above the T_g as indicated by the unchanging $\tan \delta$ curve.

185 The unconstrained shape memory capability of the tBA-co-PEGDMA and
186 tBA90/PEGDMA10 BTBD networks was evaluated using a customised platform consisting
187 of a hotplate, a glass enclosure and a temperature probe (Fig. 2). The hotplate was pre-heated
188 to a temperature that was 10°C above the highest T_g of the samples under study, i.e. $T_{\text{high}} =$
189 $(T_g + 10^\circ\text{C})$. The sample, $40 \times 20 \times 0.5 \text{ mm}^3$, was placed inside the enclosure for 10 mins to
190 equilibrate at the T_{high} temperature. The sample was deformed, θ_{Max} , using a 250 g preheated
191 steel weight and maintained at T_{high} in the enclosure, for an additional 5 mins while the
192 sample was under strain, i.e. a fixed compression stress. The sample and the weight were
193 taken from the enclosure and cooled to $3 \pm 2^\circ\text{C}$, T_{low} , in a fridge. At T_{low} the external force was
194 removed and the fixed deformability, θ_{Fixed} , was recorded. The sample was placed inside the
195 heated glass enclosure, still at T_{high} , and the recovery angles, $\theta_i(t)$, that occurred during the
196 shape memory evaluation were determined from still photographs captured, at appropriate
197 time intervals, from video recordings. Once the sample had completed its transformation
198 towards its permanent shape the value of θ_{Final} was recorded. Three replicate assessments of
199 each sample were collected and the reproducibility was such that the data point size (in
200 [Figures Figs. 6, 9 and 10](#)) covers the sample to sample variation.

201 The unconstrained shape memory effect of uncoated PET and the coated PET samples, $60 \times$
202 $20 \times 0.03 \text{ mm}^3$, was determined by cutting slits in the flat samples (Fig. 3a) and placing them
203 in the heated enclosure for 10 mins to equilibrate at the deformation temperature. They were

204 then deformed by inserting a cylindrical steel rod between the alternate strips of coated, or
 205 uncoated, PET (Fig. 3b). The deformed sample was then cooled in a fridge before the steel
 206 rod was removed and the sample placed in the chamber at T_{high} . The initial parameters noted
 207 were θ_{max} and θ_{Fixed} . A θ_{max} value of 100% reflected the ability of the sample to completely
 208 adopt the temporary shape under the influence of the deformation stress. If the sample
 209 relaxed after the stress was removed then this was recorded as θ_{Fixed} . Once these two initial
 210 parameters had been recorded a standard unconstrained shape memory evaluation was carried
 211 out with $\theta_i(t)$ being recorded photographically, as described above, every 30 seconds. When
 212 the sample transformation was complete, or the original shape recovered, θ_{Final} was recorded.
 213 The parameters extracted from the $\theta_i(t)$ versus time plot were $\theta_{1/2 Final}$ Time, i.e. the time taken
 214 to recover 50% of the permanent shape, and θ_{Final} Time, the time taken to reach θ_{Final} i.e. the
 215 time taken to return to the permanent shape.



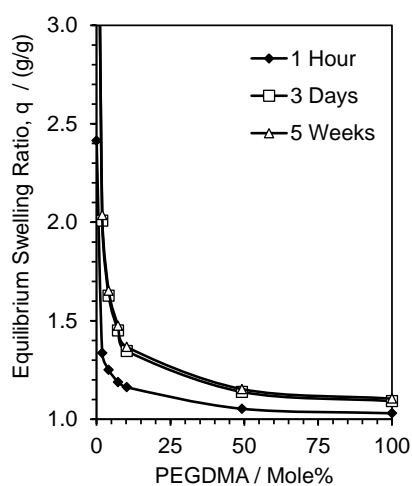
216
 217 **Fig. 3.** Schematic illustration of the cylindrical deformation method for coated PET samples.

218 **3. Results**

219 *3.1 Initial observations.*

220 The complete absence of three diagnostic absorbance bands in the FTIR spectrum of tBA,
 221 assigned to C=C stretch (ca. 1636 and 1620 cm^{-1}) and the C=CH₂ twist (ca. 811 cm^{-1})
 222 following photopolymerisation, together with the DSC data, confirmed that the reaction was

223 complete (Warren et al., 2010). As the cross link density increases a polymer becomes
224 increasingly less able to swell and the level of equilibrium swelling, q , decreases (Ortega et
225 al., 2008; Smith et al., 2009a+10; Warren et al., 2010). Linear tBA, t100/P0, completely
226 dissolved in propan-2-ol in a matter of hours indicating a complete absence of covalent cross-
227 links. The equilibrium swelling ratios, q , for the networks, t90/P10 to t0/P100, in propan-2-ol
228 decreased as the amount of PEGDMA, the cross-linking agent, increased (Fig. 4) confirming
229 that the covalent cross-links acted to prevent polymer expansion and swelling.

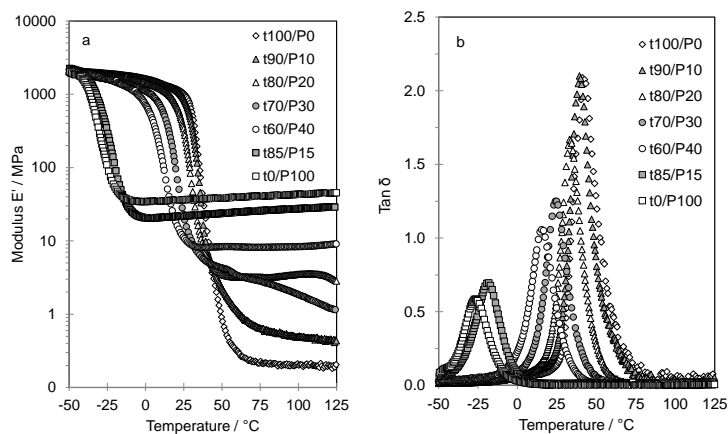


230
231 **Fig. 4.** Illustrative examples of the equilibrium swelling ratios, q , as a function of the mole
232 percent of PEGDMA after 1 h, 3 days and 5 weeks immersion in propan-2-ol.

233 3.2 Shape memory behaviour of clay-free acrylate systems

234 3.2.1 Dynamic mechanical analysis

235 The temperature variation of the storage modulus and $\tan \delta$, of the t100/P0 to t0/P100
236 samples, were plotted as a function of temperature, -50 to 125°C (Fig. 5), and the relevant
237 dynamic mechanical properties are summarized in Table 2.



238

239 **Fig. 5.** Temperature dependence of a) storage modulus, and b) $\tan \delta$ for the t100/P0 to
 240 t0/P100 networks over the temperature range -50 to 125°C.

241 Fig. 5a shows that the storage modulus at -50°C increased as the PEGDMA content increased

242 (Table 2) as did the rubbery modulus (at ca. 100°C), whereas Fig. 5b shows that both the

243 temperature at which the maximum in $\tan \delta$ occurred, and the associated peak intensity,

244 decreased with increased PEGDMA content. The temperature at which the modulus dropped

245 sharply marked the onset of the T_{ga} transition, when large segments of the polymer chains

246 gain sufficient thermal energy to begin moving, and established the starting point of the shape

247 memory effect. Tsai et al., (2008) suggested that a sharp, at least one order of magnitude,

248 decrease in storage modulus provides convincing evidence that a polymer system will

249 demonstrate shape memory capability (Du and Zhang, 2010). The temperature at which the

250 $\tan \delta_{\max}$ for a particular sample occurred (Fig. 5b) was used to define the T_g of the polymer

251 system under investigation, while the intensity and shape of the $\tan \delta$ peak provided

252 information concerning the nature of the transformation from the temporary to the permanent

253 shape. A sharp, intense $\tan \delta_{\max}$ peak followed by a reduction in $\tan \delta$ to values below 0.5

254 indicates that a SMP will behave in a manner similar to an elastomer and display significant

255 shape recovery when evaluated. In contrast, a low intensity $\tan \delta_{\max}$ indicates that a lesser

256 shape recovery will occur (Chun et al., 2002, Tsai et al., 2008). Hence, a narrow, intense $\tan \delta$

257 peak indicates a fast transformation whereas a weak broad peak suggests that the
258 transformation will be slower. A large, steep drop in storage modulus indicates that the
259 energy stored in the deformation process will enable the SMP to exert a strong physical force
260 as it returns to its permanent shape. This ability is particularly useful when the SMP has to
261 work against an opposing force such as when used as a stent where it has to open up a
262 collapsed blood vessel and keep it open (Ratna and Karger-Kocsis, 2008). Alternatively,
263 when used as a suture it may be required to contract and in so doing pull two pieces of flesh
264 together (Liu et al., 2009).

265 The initial storage modulus of the pure PEGDMA, t0/P100 (\square , Fig. 5a), was 2129 MPa at -
266 50°C and this steadily decreased reaching a value of 1903 MPa at -47°C. The T_g of this
267 system was -26°C at which point the $\tan \delta_{\max}$ value was 0.6 $\tan \delta$ (Fig. 5b). This latter value
268 was sufficient to indicate that pure PEGDMA would exhibit shape memory capability, while
269 the return to a $\tan \delta$ of ca. 0 after the transition indicated that it should also behave like an
270 elastomer. The reduction in modulus of the t0/P100 network was close to one and a half
271 orders of magnitude, from 2129 MPa at -50°C to 34 MPa at the end of the $T_{g\alpha}$ transition. The
272 gradual increase in the storage modulus to 42 MPa after the transition stage was attributed to
273 thermally induced crystallisation (Smith et al., 2009[a](#), [b](#)). Overall, pure PEGDMA (t0/P100)
274 was predicted to exhibit some useful shape memory properties.

275 At -50 °C pure tBA, t100/P0, exhibited an initial storage modulus of ca. 2005 MPa (\diamond , Fig.
276 5a) which decreased steadily until ca. +22°C, when the modulus had reached ca. 1145 MPa.
277 The narrow, high intensity $\tan \delta_{\max}$ value, of 2.1 $\tan \delta$, together with the return back to a $\tan \delta$
278 value of zero (Fig. 5b), indicated that pure tBA would behave like an elastomer and display
279 significant shape recovery when evaluated. At $\tan \delta_{\max}$ (41°C) the modulus had reduced to ca.
280 22 MPa, and continued to decrease steadily until at the end of the $T_{g\alpha}$ transition it had reached

281 ca. 0.2 MPa. The drop in pure tBA storage modulus was almost four orders of magnitude; i.e.
 282 a very strong indication of a useful shape memory capability (Tsai et al., 2008).

283 **Table 2.**
 284 Summary of the values obtained from dynamic mechanical analysis for the t100/P0 to
 285 t0/P100 networks over the temperature range -50 to 90°C.

Sample notation	Storage Modulus / MPa								$T_{g\alpha}$ / °C	Tan δ_{\max}
	-50°C	-30°C	-10°C	10°C	30°C	50°C	70°C	90°C		
t100/P0	2005	1756	1605	1368	637	0.8	0.2	0.2	41	2.1
t90/P10	2108	1961	1782	1416	425	2	0.7	0.5	39	2.1
t80/P20	2035	1847	1597	1194	61	4	3	3	33	1.7
t70/P30	1923	1688	1342	659	10	4	3	2	24	1.3
t60/P40	2168	1719	1194	160	9	8	8	8	15	1.1
t15/P85	2249	759	27	21	22	24	25	27	-18	0.7
t0/P100	2129	292	36	35	37	39	41	42	-26	0.6

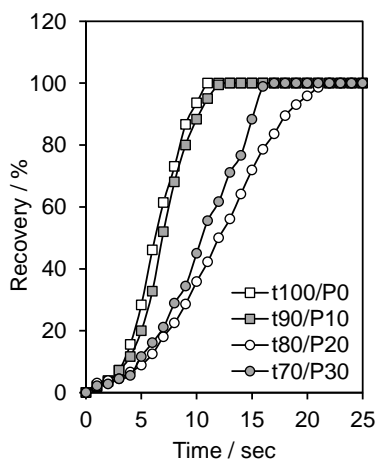
286
 287 The systems with the more intense tan δ_{\max} values, i.e. t90/P10 to t60/P40 (Table 2), were
 288 anticipated to exhibit significant shape recovery when evaluated whereas the lower tan δ_{\max}
 289 value for the t15/P85 network (0.7 tan δ), offered a clear evidence that the shape recovery
 290 would be less dramatic (Chun et al., 2002, Tsai et al., 2008). Note that the 100-fold reduction
 291 in the storage modulus of the t90/P10 to t15/P15 networks provided good evidence for useful
 292 shape memory ability (Tsai et al., 2008, Du and Zhang, 2010). The increase in storage
 293 modulus as the PEGDMA content increased was anticipated as was the associated increase in
 294 the rubbery modulus (Kramer et al., 2010).

295 Overall the storage modulus, rubbery modulus and tan δ results, suggested that addition of
 296 PEGDMA to tBA resulted in a controllable shift, to lower temperatures, of the T_g and a
 297 reduction in the tan δ_{\max} peak intensity. The rubbery storage modulus increased as the
 298 PEGDMA content increased in line with work with related systems (Gall et al., 2005; Ortega
 299 et al., 2008; Kramer et al., 2010).

300 3.2.2 Evaluation of the unconstrained shape memory effect

301 Unconstrained shape memory evaluation was employed to determine the extent to which each
302 network would demonstrate shape memory and to explore the effect of increasing PEGDMA
303 content on the speed and extent of shape reversal (Fig. 6). Cross-linked tBA-co-PEGDMA
304 polymer networks are a class I type SMP, with a $T_{trans} = T_g$ (Liu et al., 2007). An appropriate
305 SME temperature range to account for the different T_g values, which range from -26°C for
306 pure PEGDMA to $+41^{\circ}\text{C}$ for pure tBA (Table 2), needed to be identified and a T_{high} value of
307 50°C , which was 10°C above the highest T_g , was chosen to ensure full shape recovery in all
308 the relevant samples. Each network was annealed at 70°C for 15 mins prior to being
309 deformed (Table 3).

310 Due to the higher PEGDMA, and hence cross-link, content the t60/P40 and t15/P85 networks
311 were too brittle for an effective shape memory evaluation. The increased cross-link density
312 most likely caused the stress-strain behaviour of the material to change from an elastomeric
313 response to a stiff network with a pronounced brittle response (Ortega et al., 2008). The
314 t100/P0 network exhibited a θ_{Max} of 100 % (Table 3), demonstrating that it was elastic
315 enough to accommodate a high level of deformation stress. No recovery was observed after
316 the deformation constraint was removed, thus a θ_{Fixed} value of 100 % was assigned, which
317 demonstrated that the t100/P0 material could easily store the full amount of imparted strain.
318 Yang et al. (2007) reported that at low temperatures, i.e. T_{low} , the entropy driven strain
319 recovery forces are simply not sufficient to overcome the barrier to shape recovery.
320 Consequently, the deformation cannot recover while the sample is maintained at T_{low} , even at
321 long times, because the activation energy required to initiate recovery cannot be achieved.



322

323 **Fig. 6.** Unconstrained recovery of the tBA-co-PEGDMA networks, from temporary shape to
 324 permanent shape, plotted against time at a fixed temperature, 50°C.

325 Shape memory recovery was carried out at 50°C and the recovery angle, $\theta_{i(t)}$, was recorded
 326 until the pure tBA reached a θ_{Final} of 100% (Fig. 6) which demonstrated that tBA was able to
 327 store the deformed strain at T_{low} , and return to its original shape. This agreed with literature
 328 predictions, (Ortega et al., 2008), in that low, possibly negligible, cross-link density should
 329 produce a SMP with a large recoverable strain but very little ability to generate force. The $\theta_{1/2}$
 330 θ_{Final} and θ_{Final} Times of recovery, ca. 6 and 11 seconds, respectively, demonstrated that the
 331 t100/P0 network recovered ca. 50 % of its permanent shape in ca. half of the time required to
 332 return to its permanent shape.

333 The t90/P10 to t70/P30 networks also displayed a θ_{Max} of 100 % indicating that although the
 334 PEGDMA content, and therefore the number of cross-links, had increased [this did not](#)
 335 [increase neither](#) the elasticity nor [impair](#) the ability to accommodate a high level of
 336 deformation strain [had been impaired](#). The θ_{Fixed} value was 100 % for all networks, t90/P10 to
 337 t70/P30, which indicated that increasing the PEGDMA content to 30 mass% did not diminish
 338 the network's ability to retain its temporary shape at T_{low} . The t90/P10 to t70/P30 networks
 339 demonstrated, by achieving a θ_{Final} of 100 %, that they were also capable of storing the
 340 deformed strain at T_{low} and could then return to their original shape. These networks also

341 behaved as anticipated, based on the DMA results (Fig. 6), which identified the propensity
 342 for large recoverable strains (Ortega et al., 2008). The $\theta_{1/2 \text{ Final}}$ and θ_{Final} Times of recovery
 343 (Table 3) demonstrated that the t90/P10 to t70/P30 networks also recovered 50 % of their
 344 permanent shape in ca. half the full recovery time.

345 **Table 3.**

346 Values, obtained using a T_{high} of 50°C, for the parameters θ_{Max} , θ_{Fixed} , $\theta_{1/2 \text{ Final}}$, θ_{Final} , $\theta_{1/2 \text{ Final}}$
 347 Time, and θ_{Final} Time, which describe the recovery from temporary to permanent shape, for
 348 the samples described in Table 1.

Sample Description	Sample notation in figures	θ_{Max} / %	θ_{Fixed} / %	$\theta_{1/2 \text{ Final}}$ / %	θ_{Final} / %	$\theta_{1/2 \text{ Final}}$ Time / sec	θ_{Final} Time / sec
tBA100/PEGDMA0	t100/P0	100	100	50	100	6	11
tBA90/PEGDMA10	t90/P10	100	100	50	100	7	13
tBA80/PEGDMA20	t80/P20	100	100	50	100	12	22
tBA70/PEGDMA30	t70/P30	100	100	50	100	10	17
tBA90/PEGDMA10/BTBD 0	t90/P10/BTBD 0	100	100	50	100	7	12
tBA90/PEGDMA10/BTBD 1	t90/P10/BTBD 1	100	100	50	100	2.5	5.5
tBA90/PEGDMA10/BTBD 3	t90/P10/BTBD 3	100	100	50	100	4	9
tBA90/PEGDMA10/BTBD 5	t90/P10/BTBD 5	100	100	50	100	5	13
tBA90/PEGDMA10/BTBD 0 P	t90/P10/BTBD 0 P	100	93	41.5	90	52	540
tBA90/PEGDMA10/BTBD 1 P	t90/P10/BTBD 1 P	100	80	38.0	96	18	270

349
 350 Overall these results indicated that as the PEGDMA content increased there was a
 351 corresponding increase in the $\theta_{1/2 \text{ Final}}$ and θ_{Final} Times of recovery. The t70/P30 network
 352 demonstrated faster $\theta_{1/2 \text{ Final}}$ and θ_{Final} Times of recovery than the t80/P20 network which may
 353 have its origins in that the increased number of cross-links could have enabled it to store
 354 larger amounts of energy culminating in a faster response. A complete assessment of the
 355 shape memory ability of the entire t100/P0 to t0/P100 system was not possible because of the
 356 brittleness of the t15/P85 and t0/P100 networks, but, it is almost certain that their shape
 357 recovery ability would be lower because highly cross-linked networks generally demonstrate
 358 low recoverable strain (Ortega et al., 2008). In effect these observations correspond well with

359 the DMA results which identified those networks with the ability to recover their permanent
360 shape and exhibit large recoverable strains.

361 *3.2.3 Summary of clay-free acrylate networks*

362 The tBA-co-PEGDMA networks were fully cured and thermally stable, offering useful
363 mechanical properties with most of the investigated combinations able to provide a shape
364 memory response. Networks with high PEGDMA contents exhibited poor shape memory
365 properties, being brittle and fracturing when subjected to large deformations. The t90/P10
366 network showed the most promise because it could be fully polymerised, offered useful
367 mechanical properties, with similar elasticity and shape recovery capability to pure tBA, and
368 had a rubbery modulus (above its T_g) capable of withstanding moderate mechanical load.
369 However, even though this system returned to its permanent shape in only 13 ~~seconds~~, it still
370 exhibited relatively poor mechanical strength when compared to shape memory metal alloys
371 (Lin [and Wuet al.](#), 1992); a classic shortcoming of SMPs. The incorporation of well dispersed
372 OC is known to enhance the mechanical properties of acrylate networks (Wu et al., 2010;
373 Ingram et al., 2008; Oral et al., 2009) but the effect of clay incorporation on the shape
374 memory properties has not previously been explored. Consequently, the consequences of
375 adding BTBD to the t90/P10 system were investigated.

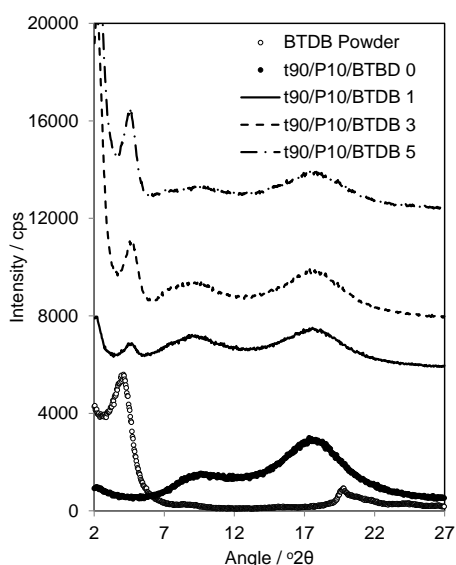
376 *3.3 Shape memory behaviour of clay-acrylate nanocomposites*

377 *3.3.1 Initial observations*

378 Swelling tests were carried out and ATR-FTIR spectra collected, as described in 3.2.1 above,
379 which confirmed that the polymer networks had fully cured and formed cross-links and that
380 all the BTBD-containing networks displayed similar swelling properties to the equivalent
381 pure polymer (Fig. 4).

382 *3.3.2 X-ray diffraction data for shape memory nanocomposites.*

383 The XRD trace for BTBD powder (Fig. 7) displayed diffraction peaks at $4.2^\circ 2\theta$ (21.0
 384 \AA), $19.7^\circ 2\theta$ (4.5\AA), and $35.0^\circ 2\theta$ (2.6\AA) which correspond to (001), (110,020) and (130,
 385 200) reflections, respectively. The trace for the sample prepared without clay (t90/P10/BTBD
 386 0) showed two broad reflections at $9.1^\circ 2\theta$ (9.7\AA) and $17.5^\circ 2\theta$ (5.1\AA) which were attributed
 387 to the polymer. The XRD traces for the systems containing 1, 3 and 5 mass% BTBD
 388 (t90/P10/BTBD 1, 3 and 5) all displayed a single peak at $4.5^\circ 2\theta$ (19.6\AA) as well as the two
 389 reflections associated with the polymer, at $9.5^\circ 2\theta$ (9.7\AA) and $17.5^\circ 2\theta$ (5.1\AA). The
 390 diffraction peaks associated with BTBD at $19.7^\circ 2\theta$ (4.5\AA) and $35.0^\circ 2\theta$ (2.6\AA) were too
 391 weak to be seen at these addition levels.



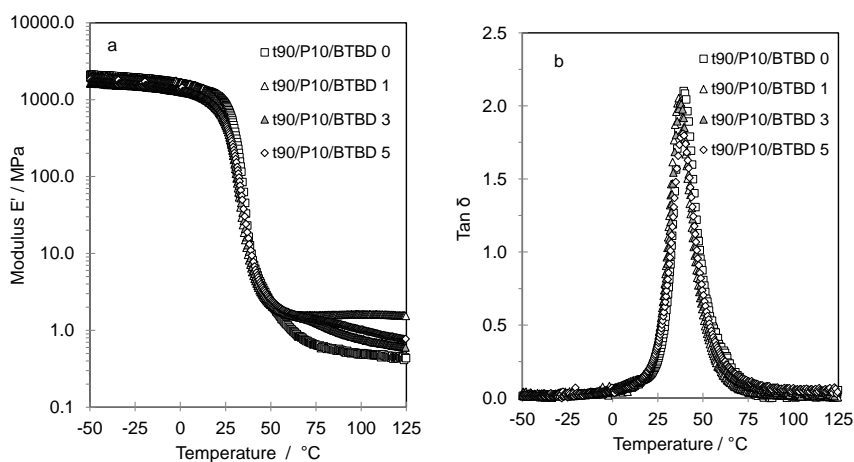
392
 393 **Fig. 7.** Cu XRD traces of BTBD and the t90/P10/BTBD 0 to 5 networks.

394
 395 The low angle reflection associated with BTBD, in the BTBD-containing networks, appeared
 396 at slightly higher angles than that of the BTBD powder (Fig. 7). Vaia and Liu (2002) have
 397 advised caution when tempted to overstate the consequences of small shifts in the positions of
 398 reflections in CPN, because several factors can contribute to a decrease in diffraction peak

399 intensity and uncertainty concerning the distance between the layers. The apparent reduction
400 in basal spacing from 21.0 to 19.6 Å could indicate a reduction in the interlayer content but a
401 more likely explanation, in accord with Vaia and Liu's interpretation, is that the shift arises
402 from a change in the number of layers per stack and angular variations between layers in a
403 stack. Nonetheless, the diffraction data confirmed that polymerisation did not occur, nor was
404 polyacrylate present, in the interlayer space. The apparent absence of poly(tBA-co-
405 PEGDMA) in the interlayer contrasts with the report of Ingram et al., (2008) who found that
406 quaternary (bis-2-hydroxyethyl) methyl tallowammonium-exchanged Cloisite, C30B, formed
407 exfoliated/intercalated CPN in a radically-initiated methylmethacrylate (MMA) network. The
408 XRD trace for MMA containing 1 and 2 mass% C30B exhibited no diffraction peaks leading
409 the authors to suggest full exfoliation, whereas the XRD trace for the 4 mass% 30B/MMA
410 sample displayed a reflection at $2.1^\circ 2\theta$ (42.0 Å) indicating [that](#) an intercalated CPN had been
411 produced.

412 | 3.3.2.3 *Dynamic mechanical analysis of clay-acrylate nanocomposites*

413 The storage modulus and $\tan \delta$ values, for the t90/P10/BTBD 0 to 5 networks, are plotted in
414 Fig. 8 over the temperature range, -50 to +125°C, and the associated values for the properties
415 of interest are summarised in Table 4. The data for the t90/P10/BTBD 0 sample was
416 described above (t90/P10, Fig. 5, Table 2) and the samples prepared by incorporation of
417 BTDB into this host matrix, t90/P10/BTBD 1 to 5, exhibited initial storage moduli of ca.
418 1949, 1629 and 1702 MPa, respectively, at -50°C which steadily decreased reaching values
419 of ca. 1417, 1040 and 1083 MPa at 12°C. The ensuing steep drop in the moduli established
420 the starting point of the shape memory effect and resulted in reductions of at least three and a
421 half orders of magnitude in modulus, reaching 1.0, 0.5 and 0.6 MPa, respectively, at 150°C.



422

423 **Fig. 8.** Temperature dependence of a) storage modulus, b) $\tan \delta$ of the t90/P10/BTBD 0 to 5
 424 networks over the temperature range -50 to 125°C.

425 The T_g values for the t90/P10/BTBD 1, 3 and 5 samples were very similar at 37, 37 and 38°C,
 426 respectively. The corresponding $\tan \delta_{\max}$ values, 2.1, 2.0 and 1.8 $\tan \delta$, taken together with the
 427 reduction in the associated $\tan \delta$ values to zero, were large enough to confidently predict that
 428 these networks would display elastomeric behaviour and exhibit useful shape memory
 429 properties. However, these results were remarkably similar to the t90/P10 host polymer so no
 430 dramatic increase in shape memory capability was expected.

431 **Table 4.**

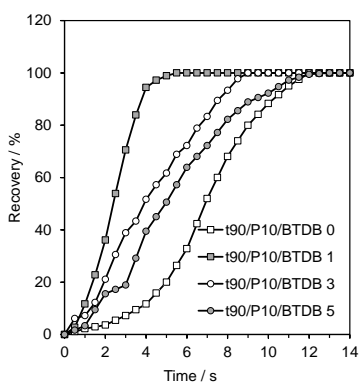
432 Summary of the values obtained from dynamic mechanical analysis for the t90/P10/BTBD 0
 433 to 5 networks over the temperature range -50 to 150°C.

Sample Description	Storage Modulus / MPa							T_g / °C	Tan δ_{\max}
	-50°C	-25°C	0°C	25°C	50°C	100°C	150°C		
t90/P10/BTBD 0	2108	1928	1629	876	2	0.5	0.4	40	2.1
t90/P10/BTBD 1	1949	1808	1563	549	2	2.0	1.0	37	2.1
t90/P10/BTBD 3	1629	1562	1276	459	2	0.8	0.5	37	2.0
t90/P10/BTBD 5	1702	1564	1322	508	3	1.0	0.6	38	1.8

434

435 The DMA results confirmed that the incorporation of BTBD resulted in no significant shift of
 436 the T_g and only small reductions in the $\tan \delta_{\max}$ peak intensity; as noted for shape memory

437 clay-epoxy nanocomposites (Liu et al., 2011). The rubbery modulus of the t90/P10/BTBD 1
 438 network was more than twice that of the other, clay-containing, networks indicating that it
 439 could maintain greater mechanical loading than the other systems when $T > T_g$. Benfarhi et al.
 440 (2004) and Okamoto et al. (2000) also noted that the highest modulus was obtained with a
 441 clay loading of ca. 1 mass% in related, non-SMP, acrylate CPN. However, as the BTBD
 442 content was increased the initial storage modulus decreased from that of the host matrix
 443 which corresponded to reports where acrylate networks, PU-based acrylates and epoxy-based
 444 acrylates, exhibited a drop in initial storage modulus with increasing clay content (Benfarhi et
 445 al., 2004; Keller et al., 2004). It is, however, more common for the initial storage modulus to
 446 increase when the OC is effectively dispersed throughout the polymer matrix(Okamoto et al.,
 447 2001; Shemper et al., 2004; Decker et al., 2005; Xu et al., 2006; Zang et al., 2009).



448
 449 **Fig. 9.** Unconstrained SME testing of t90/P10/BTBD 0 to 5 networks, from temporary to
 450 permanent shape, plotted against time at a fixed temperature, 50°C.

451 3.3.34 *Evaluation of the unconstrained shape memory effect*

452 The unconstrained shape memory ability was evaluated to establish whether the BTBD-
 453 containing networks would demonstrate shape memory and to determine the effect of BTBD
 454 content (Fig. 9). The close proximity of the T_g values for the different samples meant that a
 455 single deformation regime was appropriate. Table 3 summarises the properties of interest.

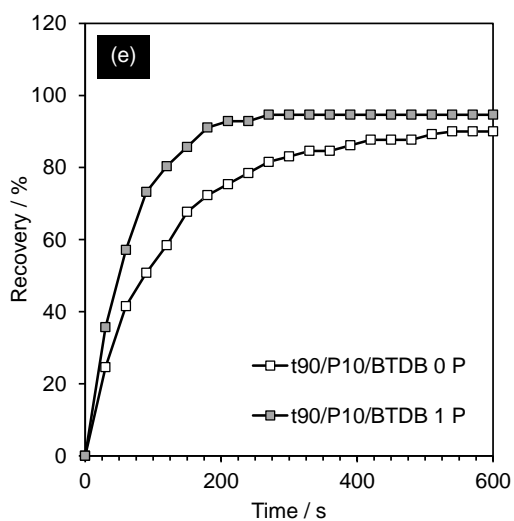
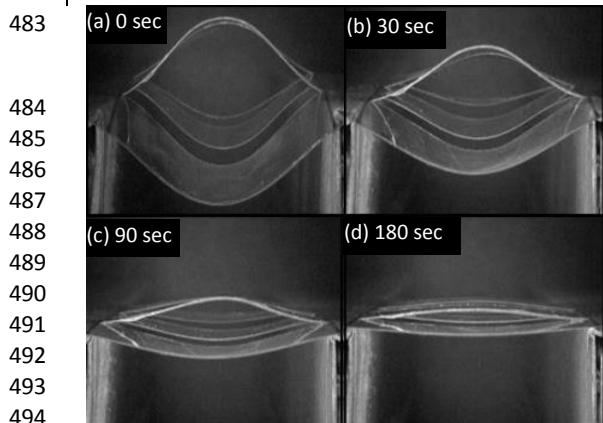
456

457 Once again the values of θ_{Final} , $\theta_{1/2 \text{ Final}}$ Time and θ_{Final} Time (Fig. 9, Table 3) confirmed that
458 the clay-free network stored the full load of imposed strain and that it recovered 50% of its
459 permanent shape in half the time required for full recovery. The t90/P10/BTBD networks also
460 displayed a θ_{Max} of 100 %, confirming that the BTBD content did not retard the elasticity nor
461 reduce the networks' ability to accommodate a high level of deformation strain. The θ_{Fixed}
462 results were also 100 % for all these systems confirming that an increased BTBD content did
463 not diminish the ability of the networks to retain their temporary shape. Reaching a θ_{Final} of
464 100 % proved that these networks could store the deformed strain and return to their
465 permanent shape. The $\theta_{1/2 \text{ Final}}$ and θ_{Final} Times of recovery (Table 3) demonstrated that the
466 BTBD-containing samples also recovered 50 % of their permanent shape in ca. half the full
467 recovery time. Most of these observations corresponded well with the results predicted by
468 DMA, but the DMA data was singularly unable to predict the extent to which the presence of
469 BTBD accelerated the rate of permanent shape recovery. The fastest return to the permanent
470 shape was achieved when 1 mass% BTBD was incorporated. Liu et al. (2011) also observed
471 that the θ_{Final} Times of recovery for clay-epoxy [SMPSMPs](#) did not vary systematically with
472 OC content and the shortest recovery time occurred when 3 mass% of a
473 cetyltrimethylammonium-clay was used. The authors attributed this non-systematic variation
474 to a reduction in OC dispersion at loadings of 4 and 5 mass%.

475 | 3.3.45 *Imparting shape memory effect to PET film*

476 The t90/P10/BTBD 1 network demonstrated the fastest return to its permanent shape and
477 exhibited the largest rubbery modulus (2.0 MPa) so it was chosen as the preferred system to
478 coat onto a PET substrate. The aim was to determine whether this acrylate network could
479 confer shape memory capability to the PET substrate and whether the presence of BTBD
480 offered any additional capability (Fig. 10). The t90/P10/BTBD 0 and 1 coated PET substrate

481 and uncoated PET sheet were deformed, after annealing at 70°C, and their shape memory
482 recoveries determined as described in [Section 2.4](#) (Fig. 2 and 3).



497 **Fig. 10.** Unconstrained SME testing of t90/P10/BTDB 0 and 1 coated PET substrates, from
498 temporary to permanent shape. Video capture images of a t90/P10/BTDB 1 SMP coated PET
499 at sequential time intervals (a) 0, (b) 30, (c) 90 and (d) 180 sec; (e) recovery % against time.
500 All data [were](#) obtained at a fixed temperature, 50°C.

501

502 The uncoated PET sample was deformed to a θ_{Max} of 100 % (Fig. 3) and cooled to T_{low} , 0 to
503 5°C. Upon removal of the steel rod the uncoated PET sample immediately collapsed;

504 dramatically demonstrating a θ_{Fixed} value of 0 %. The t90/P10/BTBD 0 coated substrate was
505 deformed in the same manner and achieved a θ_{Max} of 100 % demonstrating that the shape
506 memory coating had accommodated the deformation stress but the sample relaxed a little at
507 T_{low} leading to a θ_{Fixed} value of 93 %. This confirmed that the t90/P10/BTBD 0 P coated
508 substrate could be deformed to a large degree and was able to store the majority of the
509 imposed strain, in marked contrast to the behaviour of the uncoated PET which collapsed
510 back to its permanent (flat) shape when the steel rod was removed. The t90/P10/BTBD 0 P
511 sample reached an ultimate recovery, θ_{Final} , of 90 % with corresponding $\theta_{1/2 \text{ Final}}$ and θ_{Final}
512 Times of 90 and 540 seconds, respectively, showing that the t90/P10/BTBD 0 P coated
513 substrate recovered 50 % of the θ_{Final} very rapidly compared to the full recovery time.

514 The t90/P10/BTBD 1 P coated substrate exhibited a θ_{Max} of 100 % and a θ_{Fixed} of 80 %
515 proving that it was also able to accommodate, and store, a high level of deformation stress,
516 albeit less than the pure acrylate coated substrate. The t90/P10/BTBD 1 coated PET substrate
517 achieved a θ_{Final} of 96 % which demonstrated that neither the t90/P10/BTBD 0 nor
518 t90/P10/BTBD 1 coated PET were able to fully return to their permanent, flat shape. The
519 $\theta_{1/2 \text{ Final}}$ and θ_{Final} Times of recovery for the t90/P10/BTBD 1 P sample were 18 and 270
520 seconds, respectively, which demonstrated that the presence of as little as 1 mass% BTBD in
521 a shape memory CPN could significantly accelerate the rate of permanent shape recovery of a
522 coated substrate.

523 **4. Conclusions**

524 The tBA-co-PEGDMA crosslinked networks displayed useful shape memory properties up to
525 PEGDMA contents of 40 %. Above this PEGDMA content the materials were prone to
526 fracture and too brittle for a realistic assessment of their shape memory capability. The
527 tBA90/PEGDMA10 material was selected as the host matrix to investigate the effect of

528 incorporating OC on the shape memory capability. X-ray diffraction data confirmed that
529 BTBD formed a microcomposite in the selected matrix and hence exerted no influence on the
530 storage modulus, rubbery modulus, glass transition temperature, T_g , or the shape or intensity
531 of the $\tan \delta$ peak of the host matrix. Therefore, it was anticipated that the presence of BTBD
532 would have no effect, positive or negative, on the shape memory properties of the host
533 matrix. However, it was found that the incorporation of clay, especially at the 1 mass% level,
534 significantly accelerated the speed at which the microcomposite returned to the original,
535 permanent shape. This accelerated return to the permanent shape, compared to the clay-free
536 SMP, was also observed when the microcomposite was coated onto a 100 μm PET film.

537 **5. Acknowledgements**

538 MB gratefully acknowledges support from the Engineering and Physical Science Research
539 Council via a CASE Award (Voucher Number 08002513).

540

541 **References**

- 542 Annabi-Bergaya F., 2008. Layered clay minerals. Basic research and innovative composite
543 applications. *Microporous and Mesoporous Mater.* 107, 141-148.
- 544 Behl M., Razzaq M.Y., Lendlein A., 2010. Multifunctional Shape-Memory Polymers. *Adv.*
545 *Mater.* 22, 3388-3410.
- 546 Benfarhi S., Decker C., Keller L., Zahouily K., 2004. Synthesis of clay nanocomposite
547 materials by light-induced crosslinking polymerization. *Eur. Polym. J.* 40, 493-501.
- 548 Cao F., Jana S.C., 2007. Nanoclay-tethered shape memory polyurethane nanocomposites.
549 *Polymer.* 48, 3790-3800.
- 550 Chun B.C., Cha S.H., Chung Y.C., Cho J.W., 2002. Enhanced dynamic mechanical and
551 shape-memory properties of a poly(ethylene terephthalate)-poly(ethylene glycol)
552 copolymer crosslinked by maleic anhydride. *J. Appl. Polym. Sci.* 83, 27-37.
- 553 Chung Y-C., Choi J.W., Park J.S., Shin C.H., Chun B.C., 2011. Covalent bonding of surface-
554 modified montmorillonite nanoparticle with polyurethane and its impact on shape
555 memory effect and mechanical properties. *J. Thermoplastic Composite Materials.* 24, 477-
556 497.
- 557 Decker C., Keller L., Zahouily K., Benfarhi S., 2005. Synthesis of nanocomposite polymers
558 by UV-radiation curing. *Polymer.* 46, 6640-6648.
- 559 Du H.Y., Zhang J.H., 2010. Shape memory polymer based on chemically cross-linked
560 poly(vinyl alcohol) containing a small number of water molecules. *Colloid. Polym. Sci.*
561 288, 15-24.
- 562 Gall K., Yakacki C.M., Liu Y.P., Shandas R., Willett N., Anseth K.S., 2005.
563 Thermomechanics of the shape memory effect in polymers for biomedical applications.
564 *J. Biomed. Mater. Res. A*, 73A, 339-348.
- 565 Ge Q., Luo X.F., Iversen C.B., Mather P.T., Dunn M.L., Qi H.J., 2013. Mechanisms of triple-
566 shape polymeric composites due to dual thermal transitions. *Soft Matter.* 9, 2212-2223.
- 567 Haghayegh M., Sadeghi G.M.M., 2012. Synthesis of shape memory polyurethane/clay
568 nanocomposites and analysis of shape memory, thermal and mechanical properties.
569 *Polym. Comp.* 843-849.
- 570 Ikematu T., Kishimoto Y., and Miyamoto K., 1993. Shape memory polymer resin
571 composition and the shape memorizing moulded product thereof. Japan Patent 5189110.
- 572 Ingram S., Dennis H., Hunter I., Liggat J.J., McAdam C., Pethrick R.A., Schaschke C.,
573 Thomson D., 2008. Influence of clay type on exfoliation, cure and physical properties of
574 in situ polymerised poly(methyl methacrylate) nanocomposites. *Polym. Int.* 57, 1118-
575 1127.
- 576 Jiang H.Y., Kelch S., and Lendlein A., 2006. Polymers move in response to light. *Adv.*
577 *Mater.* 18, 1471-1475.
- 578 Keller L., Decker C., Zahouily K., Benfarhi S., Le Meins J.M., Mieke-Brendle J., 2004.
579 Synthesis of polymer nanocomposites by UV-curing of organoclay-acrylic resins.
580 *Polymer.* 45, 7437-7447.
- 581 Kramer N.J., Sachtelben E., Ozaydin-Ince G., van de Sanden R., Gleason K.K., 2010. Shape
582 memory polymer thin films deposited by initiated chemical vapor deposition.
583 *Macromolecules.* 43, 8344-8347.

Formatted: Spanish (Spain-Traditional Sort)

Formatted: English (U.K.)

Formatted: English (U.K.)

- 584 Lendlein A., Kelch S., 2002. Shape-memory polymers. *Angew. Chem. Int. Edn.* 41, 2035-
585 2057.
- 586 Lendlein A., Langer R., 2002. Biodegradable, elastic shape-memory polymers for potential
587 biomedical applications. *Science.* 296, 1673–1676
- 588 Liff S.M., Kumar N., McKinley G.H., 2007. High-performance elastomeric nanocomposites
589 via solvent-exchange processing. *Nat. Mater.* 6, 76-83.
- 590 Lin H.C., Wu S.K., 1992. Strengthening effect on shape recovery characteristic of the
591 equiatomic TiNi alloy. *Scripta Metall.*, 26, 59–62
- 592 Liu C., Qin H., Mather P.T., 2007. Review of progress in shape-memory polymers. *J.Mater.*
593 *Chem.* 17, 1543-1558.
- 594 Liu Y., Han C., Tan H., Du X., 2011. Organic-montmorillonite modified shape memory
595 epoxy resin. 22, 2017-2021.
- 596 Liu Y.J., Lu H.B., Lan X., Leng J.S., Du S.Y., 2009. Review of electro-activate shape-
597 memory polymer composite. *Compos. Sci. Technol.* 69, 2064–2068
- 598 Maitland D. J., Metzger M. F., Schumann D., Lee A., 2002. Photothermal properties of shape
599 memory polymer micro-actuators for treating stroke. *Laser. Surg. Med.* 30, 1-11.
- 600 Migneco F., Huang, Y.C., Birla R.K., Hollister S.J., 2009. Poly(glycerol-dodecanoate), a
601 biodegradable polyester for medical devices and tissue engineering scaffolds.
602 *Biomaterials*, 30, 6479-6484.
- 603 | [Okamoto M., Morita S., Kim Y.H., Kotaka T., Tateyama H., 2001. Dispersed structure](#)
604 [change of smectic clay/poly\(methyl methacrylate\) nanocomposites by copolymerization](#)
605 [with polar comonomers. *Polymer.* 42, 1201-1206.](#)
- 606 | [Okamoto M., Morita S., Taguchi H., Kim Y.H., Kotaka T., Tateyama H., 2000. Synthesis and](#)
607 [structure of smectic clay/poly\(methyl methacrylate\) and clay/polystyrene](#)
608 [nanocomposites via in situ intercalative polymerization. *Polymer.* 41, 3887-3890.](#)
- 609 | [Oral A., Tasdelen M.A., Demirel A.L., Yagci Y., 2009. Poly\(methyl methacrylate\)/clay](#)
610 [nanocomposites by photoinitiated free radical polymerization using intercalated](#)
611 [monomer. *Polymer.* 50, 3905-3910.](#)
- 612 Ortega A.M., Kasprzak S.E., Yakacki C.M., Diani J., Greenberg A.R., Gall K., 2008.
613 Structure-property relationships in photopolymerizable polymer networks: Effect of
614 composition on the crosslinked structure and resulting thermomechanical properties of a
615 (meth)acrylate-based system. *J. Appl. Polym. Sci.* 110, 1559-1572.
- 616 Quadrini F., Santo L., Squeo E.A., 2012. Solid-state foaming of nano-clay-filled thermoset
617 foams with shape memory properties. *Polymer-Plastics Technology and Engineering* 51,
618 560-567.
- 619 | [Ratna D., Karger-Kocsis J., 2008. Recent advances in shape memory polymers and](#)
620 [composites: a review. *J. Mater. Sci.* 43, 254-269.](#)
- 621 Rezanejad R., Kokabi M., 2007. Shape memory and mechanical properties of cross-linked
622 polyethylene/clay nanocomposites. *Eur. Polym. J.* 43, 2856 -2865
- 623 Safranski D.L., Gall K., 2008. Effect of chemical structure and crosslinking density on the
624 thermo-mechanical properties and toughness of (meth)acrylate shape memory polymer
625 networks. *Polymer.* 49, 4446-4455.

Formatted: English (U.K.)

Formatted: English (U.K.)

Formatted: Spanish (Spain-Traditional Sort)

Formatted: English (U.K.)

626 Shemper B.S., Morizur J.F., Alirol M., Domenech A., Hulin V., Mathias L.J., 2004. Synthetic
627 clay nanocomposite-based coatings prepared by UV-cure photopolymerization. *J. Appl.*
628 *Polym. Sci.* 93, 1252-1263.

629 | Smith K.E., Parks S.S., Hyjek M.A., Downey S.E., Gall K., 2009^a The effect of the glass
630 transition temperature on the toughness of photopolymerizable (meth)acrylate networks
631 under physiological conditions. *Polymer.* 50, 5112-5123.

632 | Smith K.E., Temenoff J.S., Gall K., 2009^b. On the toughness of photopolymerizable
633 (meth)acrylate networks for biomedical applications. *J. Appl. Polym. Sci.* 114, 2711-
634 2722.

635 Tao X., 2010. Tunable polymer multi-shape memory effect. *Nature.* 464, 267-270

636 Tong T.H., 2004. Shape memory styrene copolymer. Patent US6759481 B2.

637 Tsai Y., Tai C.H., Tsai S.J., Tsai F.J., 2008. Shape memory effects of poly(ethylene
638 terephthalate-co-ethylene succinate) random copolymers. *Eur. Polym. J.* 44 , 550-554.

639 Utracki L.A., 2010. Clay-Containing Polymeric Nanocomposites and Their Properties. *IEEE*
640 *Electr. Insul. M.* 26, 6-15

641 Vaia R.A., Liu W.J., 2002. X-ray Powder Diffraction of Polymer/Layered Silicate
642 Nanocomposites: Model and Practice. *J. Polym. Sci. Polym. Phys.* 40, 1590-1600.

643 Venkatraman S.S., Tan L.P., Joso J.F., Boey Y.C., Wang X., 2006. Biodegradable stents with
644 elastic memory. *Biomaterials.* 27, 1573-1578

645 Voit W., Ware T., Dasari R.R., Smith P., Danz L., Simon D., Barlow S., Marder S.R., Gall
646 K., 2010. High-strain shape-memory polymers. *Adv. Funct. Mater.* 20, 162-171.

647 Warren P.D., McGrath D.V., and Geest J.P.V., 2010. Effect of crosslinker length and
648 composition on the hydrophobicity and thermomechanical response of acrylate-based
649 shape-memory polymers. *Macromol. Mater. Eng.* 295, 386-396.

650 Wu G.L., Liu G.P., Zang Y.L., Lu Y.B., Xiong Y.Q., Xu W.J., 2010. Preparation and
651 characteration of UV-cured EA/MMT nanocomposites via in-situ polymerization. *J.*
652 *Macromol. Sci. A. Pure. Appl. Chem.* 47, 647-654.

653 Wu T., O'Kelly K., Chen B., 2013. Poly(methylmethacrylate)-grafted clay-thermoplastic
654 elastomer composites with water - induced shape-memory effects. *J. Polym. Sci. Polym.*
655 *Phys.* 51, 1513-1522.

656 Xu B., Huang W.M., Pei Y.T., Chen Z.G., Kraft A., Reuben R., De Hossen J.Th.M., Fu Y.Q.
657 2009. Mechanical properties of attapulgite clay reinforced polyurethane shape-memory
658 nanocomposites. 45, 1904-1911.

659 Xu Y.J., Brittain W.J., Vaia R.A., Price G., 2006. Improving the physical properties of
660 PEA/PMMA blends by the uniform dispersion of clay platelets. *Polymer.* 47, 4564-4570.

661 Yakacki C.M., Shandas R., Safranski D., Ortega A.M., Sassaman, K., Gall K., 2008. Strong,
662 tailored, biocompatible shape-memory polymer networks. *Adv. Funct. Mater.* 18, 2428-
663 2435

664 Yang F., Wornyo E., Gall K., King W.P., 2007. Nanoscale indent formation in shape memory
665 polymers using a heated probe tip. *Nanotechnology.* 18, 285302.

666 Zang Y.L., Xu W.J., Liu G.P., Qiu D.Y., Su S.P., 2009. Preparation of ultraviolet-cured
667 bisphenol A epoxy diacrylate/montmorillonite nanocomposites with a bifunctional,
668 reactive, organically modified montmorillonite as the only initiator via in situ. *J. Appl.*
669 *Polym. Sci.* 111, 813-818.